Synthesis of palladium with different nanoscale structures by sputtering deposition onto fiber templates

Victor M. Pantojas,[a] Diego Rodríguez,[b] Gerardo Morell,[b,d] Adamari Rivera,[a] Carlos Ortiz,[a] Jorge J. Santiago-Avilés,[c] and Wilfredo Otaño[a,d]

[a] Department of Physics-Mathematics, University of Puerto Rico at Cayey, Cayey, PR 00736
[b] Department of Physics, University of Puerto Rico at Río Piedras, San Juan, PR 00931
[c] Department of Electrical Engineering, University of Pennsylvania, Philadelphia, PA 19104
[d] Institute for Functional Nanomaterials, University of Puerto Rico, San Juan, PR 00931
vpantojas@cayey.upr.edu,[a] gerardo@epscor.upr.edu,[b] Santiago@seas.upenn.edu, [c]
wilfredo.otano@upr.edu [d]

Abstract. A flexible and versatile method combining sputtering and electrospinning techniques was used to shape different palladium morphological structures with nanoscale features. The samples were prepared by dc-magnetron sputtering onto thermally degradable polymer templates. The sputtering parameters were chosen to deposit the metal under low adatom-mobility conditions. After deposition, the template was removed by heat treatment, thereby forming different palladium morphologies with shapes resembling ribbons and half tubes, amongst others. X-ray diffraction studies demonstrated that they are composed of crystalline palladium or palladium oxide, depending on the heat treatment. The cylindrical walls are composed of 30 nm or smaller crystallites, as measured from transmission electron microscopy images. A mathematical simulation demonstrate that the morphological structures obtained are a consequence of the sputtering line-of-sight deposition process. This fabrication process can be varied to modify three types of structures at the nanoscale level: the external shape, the columnar shape of the walls, and the nano-crystallinity. The external shape can be modified by controlling the deposition time and the fiber template diameter. The columnar shape of the walls and the nano-crystallinity can be modified by changes in the sputtering process parameters. The nanoscale morphologies created have potential uses in sensing and photonic applications.

Keywords: nanoscale morphology, morphological structures, crystalline structures, sputtering, electrospinning.

1 INTRODUCTION

Russell Messier and colleagues at Penn State studied the morphological structure of different materials and developed an important understanding of the morphology-characteristic-properties relationship. In physical vapor deposition (PVD) of thin films, they were able to show the impact of energetic bombardment in the development of the morphological structure of the deposited materials, thus modifying the Movchan-Demchishin [1] and Thornton [2] structure zone models [3]. The development of the columnar grain structure in sputtered films was elucidated in the deposition of amorphous and crystalline films [3]. Substrate temperature, energetic bombardment, chemistry of the species being deposited, and direction of the vapor flux being deposited with respect to the substrate normal were recognized as key processing parameters to change the morphology and crystallinity of the deposited materials [4-9]. In this article, these ideas will be used to explain the formation of morphological and crystalline structures of palladium at the nanoscale range.

Received 9 Sep 2008; accepted 10 Nov 2008; published 13 Nov 2008 [CCC: 19342608/2008/$25.00]

It is important to notice that in studies where there is an important feature at the micro and nanoscale level the word structure could refer to a crystallinity parameter or to specify an external pattern of the material, i.e. the morphology. The German root of the word morphology suggests the study of the shape or form to define a structure [10]. In materials science, at the macroscopic level, the word morphology is used to describe the external shape or form of rocks and crystals, while "internal morphology" is sometimes used by the scientific community to refer to the internal crystalline structure [11]. At the micro and nanoscale level, typically only one of these structures is being studied, crystallinity or morphology, and may not be necessary to distinguish between them. In this article both are important and, to prevent any confusion, morphological structure will be used to denote a distinctive pattern in the external shape of a material, and to distinguish it from the crystalline structure.

Morphological and crystalline structures with high surface-to-volume ratio are of interest in many technological applications. Palladium, in particular, is of considerable interest due to its potential applications in catalysis [12, 13], hydrogen storage [14] and sensing technology [15], and the use of morphological and/or crystalline nanostructures should strongly enhance the reactivity and response time for these applications [16]. Several PVD and chemical vapor deposition (CVD) methods have been used for the synthesis of palladium morphological nanostructures [17-22]. Sputtering deposition, in particular, is an interesting technique as a result of the possible control of process parameters that allows for the modification of characteristics and properties of a wide range of materials. For example, the use of low substrate temperatures and high deposition rates will produce low adatom-mobility deposition conditions which in high melting point materials will result in the synthesis of films with crystallite sizes in the nanoscale range. As shown by Messier and colleagues, the morphology of these films at the micro and nanoscale levels typically shows a characteristic columnar structure. At the microscale level different shapes of the columns have been prepared,variously described as inverted cone, fibrous or columnar grains, and matchstick [23, 24]. This micro scale morphology can be modified using the sputtering process parameters to create sculptured thin films [9].

At the nanoscale level, it is difficult to control the sputtering process parameters to create a particular morphological structure, and it is not known if this is possible independent of the material being deposited. Most methods rely in the use of additional techniques to create features at the nanoscale level that will complement the sputtering-deposition process in the formation of specific morphological structures. A successful method to produce this kind of structures relies on the use of templates which acts like molds. Molds with different shapes such as spheres, fibers or porous membranes have been used to tailor some specific morphological patterns of materials deposited using PVD and CVD methods [25-28]. The morphological structures created can be released, if desired, by eliminating the templates with a heat treatment or a dissolution process. An interesting application of this methodology is presented by Lu *et al.* [29] where they evaporate gold on top of a sacrificial-nanospheres template to create nanophotonic moon structures. These morphological structures have sharp edges that allow an increase in Raman scattering signal by several orders of magnitude. This phenomenon known as surface-enhanced Raman scattering, results in a highly specific and sensitive method for molecular identification. It is known that the sharp features in the metal nanostructure create the largest electromagnetic enhancement but is not understood how the specific shape of these features relate to the signal enhancement.

A simple method to produce templates with the shape of fibers, that are exceptionally long and uniform in diameter, is electrospinning. This technique is based on the uniaxial stretching of a viscoelastic polymer solution under the electrostatic forces on surface charges when exposed to an external electric field. The incorporation of precursors into the polymer solution for electrospinning, followed by pyrolysis to eliminate the polymer, has been used in the formation of fibers with diversified compositions [30]. In this article it is reported the use

of electrospun fibers as sacrificial templates that were coated with palladium by dc-sputtering, followed by the selective removal of the templates by heat treatment. The fibers act as molds for the fabrication of a variety of structures made of palladium where the morphology and crystallinity are controlled at the nanoscale level.

2 EXPERIMENTAL DESCRIPTION

Polyethylene oxide dissolved in a mixture of ethanol and water was used as the precursor for electrospining of the fiber template. A high voltage power supply (Gamma Research Inc.) was connected between the needle of the syringe and the collecting plate, a distance of 30 cm apart. The applied potential difference was varied between 17 and 19 kV. A piece of silicon wafer, placed in front of the collecting plate, was used as a substrate. The silicon substrate was previously cleaned with detergent, methanol and acetone. The feeding rate of the polymer solution was 0.3 mL/h. The sputtering deposition process is described elsewhere [31]. Briefly, palladium was deposited on top of the electrospun fibers template by dc magnetron sputtering of a 99.999% pure Pd target in an ultra high purity Ar gas. The deposition chamber used a turbo-molecular pump to routinely achieve base pressures below 6.6×10^{-3} Pa. The deposition pressure was set to 1.7 Pa, and the sputtering power to 50 W. A calibration curve of thickness versus time was prepared by depositing the metal on a masked silicon substrate and measuring the step created using a stylus profilometer. The deposition time was then controlled to obtain a set of samples with corresponding Pd thickness of 25 nm, 50 nm, 300 nm, 500 nm and 600 nm at a deposition rate of approximately 120 nm/min. These thicknesses represent 2.5, 5.0, 30, 50 and 60% of the mean template fiber diameter of 1 μm. The coated samples were heated at 320 ^{o}C for 2 hrs in a tubular furnace opened to air, or flushed with nitrogen, in order to gasify the polymer and remaining solvent at the lowest temperature reported in literature [32]. A JEOL JSM-6360 scanning electron microscope was used to analyze the as-spun and coated fibers. Micrographs were taken at random areas at low, medium and high magnifications and at different locations to verify that they represent the morphology of each sample. The diameters of the fibers were measured from the micrographs using commercial image analysis software. X-ray diffraction was performed with a Bruker Hi-star System with a General Area Detector (GADDS). The sample angle was set at $\omega = 20^{o}$ while the detector angle was set at $2\theta = 45^{o}$. The two dimensional diffraction frames were integrated to obtain the one-dimensional diffractogram. Transmission Electron Microscopy (TEM) was performed on a half tube sample in order to characterize the internal wall morphology.

3 RESULTS

The as-spun fibers were several cm long, continuous and with a smooth surface. The mean fiber diameter was 1 μm, as determined by analyzing the SEM micrographs. After Pd deposition and heating in air to eliminate the polymer core, the appearance of the fibers changed as shown in Fig. 1. Figs. 1(a) and 1(b) are high-magnification micrographs of the resulting morphological structures with the shape of ribbons after deposition by 12.5 s and 25 s, corresponding to Pd thickness of 25 nm and 50 nm, respectively. The typical width of the ribbons is less than 1μm, indicating that about 1/3 of the circumference of the underlying template fibers was covered with metal prior to the heat treatment. As the amount of deposited Pd increases, a larger part of the circumference is covered, as illustrated in Fig. 1(c). In this case, 300 nm of Pd (150 s) were deposited, resulting in a morphological structure similar to a half tube. For 250 s of deposition (500 nm) the metal starts to surround the underlying template fibers in several parts of the mat. This results in morphological structures similar to tubes with hollow interiors. The shape of an almost complete tube is observed in

Fig. 1(d). These morphological structures yield a high surface to volume ratio, which is ideal for gas sensing and catalytic applications.

Further increase in the amount of sputtered Pd eventually forms cylindrical fibers as shown in Fig. 1(e). For this particular sample, the electrospun polymer fibers were smaller, with an average diameter of about 250 nm, or one quarter value of the previous ones. The Pd fibers have a hollow interior after the heat treatment eliminates the polymer core (not shown). Also, as seen in Fig. 1(e), short fibers with an average diameter of 100 nm formed perpendicularly to the larger-diameter fibers. This results from the electrospinning process and it is speculated that as the solvent evaporates, and the fibers takes their final cylindrical shape, the repulsion of charges in the viscoelastic solution produces the movement of ions breaking the surface tension and resulting in the outgrowth of the smaller fibers. These secondary fibers are not seen for the case of the electrospun polymer fibers with a 1 μm average diameter that were used as templates for the fabrication of the morphological structures shown in Figs. 1 (a)-(d). The smaller secondary fibers should also be hollow, after the Pd deposition and heat treatment, but this has not been verified.

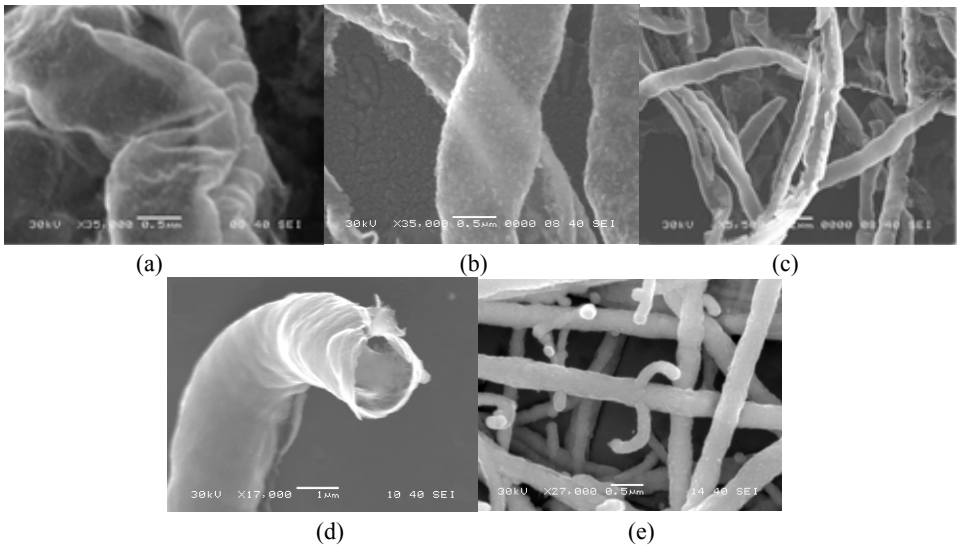

Fig. 1. SEM micrographs of Pd morphological structures where the corresponding deposition times were (a) 12.5 s, (b) 25 s, (c) 150 s, (d) 250 s and (e) 300 s. For the sample shown in (e), the mean fiber diameter previous to the Pd deposition, was 250 nm.

Figure 2 shows the resulting x-ray diffraction patterns for each morphological structure. They are crystalline and composed of pure palladium and palladium oxide (PdO). The observed peaks are identified as PdO (101) at 33.54^{o}, Pd (111) at 40.12^{o} and Pd (200) at 46.66^{o}. Palladium oxide is expected to be present as a product of oxidation during the heat treatment of the template in air. For samples with 25 nm (Fig. 2(a)) and 50 nm Pd (Fig. 2(b)) only PdO is observed, indicating that the diffusion length of the oxygen was of the order of the thickness of the deposited palladium for the chosen heating temperature and time. As the thickness of the Pd coating increases the oxidation is limited by bulk diffusion, and peaks of the crystalline Pd appear. The samples also show texture since the (200) peak of Pd should be 60 % of the highest Pd (111) peak, as indicated by the powder diffraction files [33]. For 300 nm Pd (Fig. 2(c)) the highest degree of crystal orientation is observed. This can be the result of the geometry of the half tube structure formed at 300 nm, where most of the deposited Pd lies on top of the half tube and their open part faces the substrate for the majority of them.

For the tubular morphologies formed at 500 and 600 nm, where the material is distributed around the cylindrical fibers, less crystal orientation is expected.

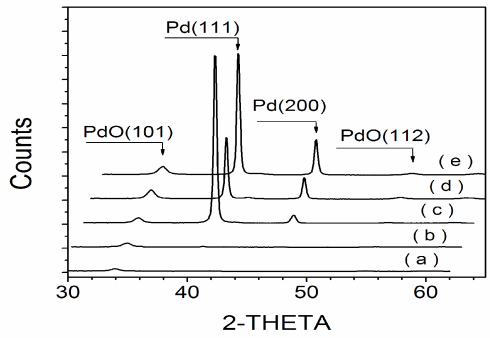

Fig. 2. Pseudo-3D representation of x-ray diffraction of the structures resulting from the deposition of different amounts of Pd on the sacrificial templates. (a) 25 nm, (b) 50 nm, (c) 300 nm, (d) 500 nm and (e) 600 nm. The graphs are displaced vertically and successively one degree in the horizontal for display.

The coated templates were also heated in an inert gas ambient in order to investigate if the decomposition of the polymer during the heat treatment plays a role in the oxidation of the Pd. Figure 3 shows the x-ray diffraction after heating the templates with the furnace (a) open to air and (b) flushed with nitrogen gas for a sample with corresponding Pd thickness of 50 nm. The oxide peaks are not observed for the case of heating in the nitrogen ambient. This demonstrates that the formation of the oxide was caused by the heat treatment and not by the degradation of the polymer.

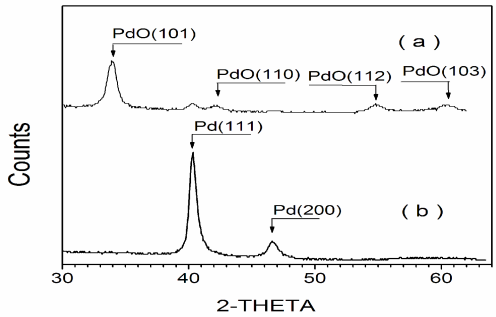

Fig. 3. X-ray diffraction of structures resulting from the deposition of 50 nm of Pd on the sacrificial templates (a) after heat treatment in air and (b) after heat treatment in ambient nitrogen.

The crystalline nanostructure was evaluated from the TEM micrographs of a sample prepared by electrospinning the polymer mat directly on top of a TEM copper grid followed by 50 s sputtering of Pd. Figure 4(a) shows the micrograph of the typical nanoscale morphology obtained after the heat treatment and Fig. 4 (b) is a cartoon of the morphology that corresponds to a half tube seen from the side to show the internal and external walls. A

high magnification of the internal wall of the tube (Fig. 4(c)) shows that they are composed of 30 nm or smaller crystallites. Small crystal sizes are expected from room temperature sputtering deposition. The low adatom-mobility conditions resulting from the low substrate temperature and high deposition rate does not allow the Pd atoms to accommodate at their thermodynamic equilibrium positions, thereby resulting in a nanoscale crystalline structure. The temperature of the heat treatment to eliminate the polymer core is small compared to the Pd melting point temperature of 1552 °C and, therefore, is not expected to affect appreciably the nanocrystals growth.

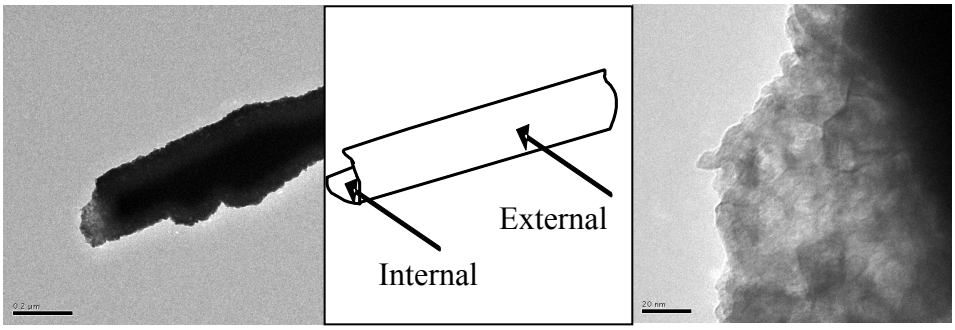

a) b) c)

Fig. 4. TEM micrographs of a Pd half tube morphological structure resulting from the deposition of Pd for 50 s onto the sacrificial templates: (a) side view of the half tube, (b) cartoon of the half tube showing the internal and external walls, and (c) magnification of the internal wall with its thickness increasing from the top to the bottom of the image.

4 DISCUSSION

At the beginning of the sputtering deposition there is not enough metal covering the fibers and silicon substrate to provide a conduction path to ground, and the substrate will develop a self-bias potential as a result of the net charge arriving to it. The difference in electrical potential between the substrate, as a result of the self-bias, and the plasma potential may produce a significant ion bombardment if the pressure is less than about 1 Pa. For higher pressures, elastic scattering between the ions and neutrals in the plasma sheath will reduce the bombardment energy, and consequently, the bombardment-induced mobility. The sputtering pressure of 1.7 Pa was chosen to be high enough to prevent significant plasma ion bombardment of the fibers and growing film but not too high to generate a large spread of this distribution of arrival angles of the material being deposited. Sputtering is a line-of-sight process where the material being deposited arrives to the growing film in a distribution of angles with a maximum in the opposite direction to the substrate normal. Scattering events between these vapor particles, moving from the target to the substrate, and the sputtering gas neutrals will spread the distribution of arrival angles as the deposition pressure is increased.

The substrate was not intentionally heated such that the deposition temperature was less than a third of the melting temperature of palladium, well within the conditions for low adatom-mobility. The result of using these plasma conditions of pressure, substrate temperature and a relatively high deposition rate is that the formation of the different morphological structures obtained by deposition onto the fibers, acting as cylindrical shape templates, can be explained to be consequence of a line of sight deposition process under low mobility conditions. Under these conditions, the shape of the coating on top of the fiber can be calculated by considering the amount of palladium deposited on an element of fiber

surface, δA_R. Following calculations presented by Westwood [23], which were based on a procedure developed by Gnaedinger [34], the flux arriving at δA_R is given by

$$d(\Delta H) = \frac{(N_0 \delta A_T \cos\theta)(\delta A_R \cos\theta)}{L^2}, \quad (1)$$

where N_0 is the number of atoms ejected along the target normal from an area element δA_T and L is the distance between the elements of surface area of the fiber δA_R and target δA_T. This expression for the flux assumes a cosθ distribution of sputtered atoms and that the target and substrate are parallel. For deposition on a cylindrical surface we introduce an angle α because different areas of the fiber surface will be at different angles with respect to the parallel position. Fig. 5 shows the geometry for the deposition. In this configuration, the projection of δA_R with respect to θ varies from α – θ, for α values between 0° to 90°, and α + θ, for negative α values up to -90°.

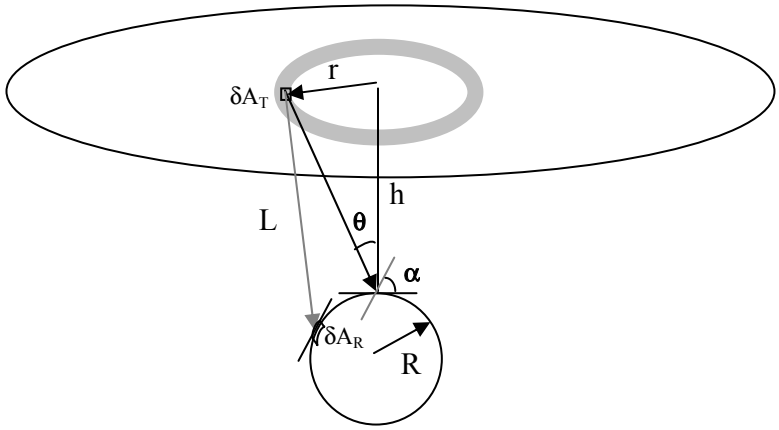

Fig. 5. Drawing of sputtering configuration showing an element of target surface δA_T, at a distance from the target center, and a circular cross-section of a cylindrical fiber of radius R(not at scale).

The equation for the flux is modified to

$$d(\Delta H) = \frac{N_0 \delta A_T \delta A_R \cos\theta[\cos(\alpha-\theta)+\cos(\alpha+\theta)]}{L^2}, \quad (2)$$

where the variables defined for α = 0° need to be modified to include variations in α according to h' = h + R (1-cosα), L' = r^2 + (h + R(1-cosα))^2, and cos θ' = h'/L'. Substituting and simplifying, we obtain

$$d(\Delta H) = \frac{2N_0 \delta A_T \delta A_R \cos\alpha h'^2}{L'^4}. \quad (3)$$

Integration for a circular annulus of the target, $\delta A_T = 2\pi r\, dr$, gives

$$\Delta H = \frac{2\pi N_0 \delta A_R R_T^{\,2} \cos\alpha}{h'^2 + R_T^{\,2}}, \tag{4}$$

where R_T is the radius of the target. For the experimental conditions used during sputtering, with the target to substrate distance h = 7.5 cm and the fiber radius R of the order of 1 μm, h >> R and h' ≈ h. Then, the variations in deposition rate, ΔH, are a consequence of the variations in the solid angle subtended at δA_T by δA_R for different α values on the surface of the fiber.

Figure 6(a) is a representation of a cross-section of the top part of a fiber (in gray) deposited with palladium. The values of ΔH were calculated for different δA_R in the surface of the fiber, corresponding to different values of α, and used to define the magnitude of a vector perpendicular to the substrate at that position. These vectors, shown in black in Fig. 6(a), create the shape of a crescent moon in cross sections and a half tube in three dimensions. The thickness of the Pd shell is a maximum at the top of the fiber, where α = 0, and decreases symmetrically to each side following the cosα function. Heating the fibers, to eliminate the central polymer core (fugitive phase), results in the formation the Pd tube shape where at the edges the wall thickness decreases. Figure 6(b) is a micrograph of a morphological structure with a similar shape to the one predicted by the model. The asymmetry of the deposition is evident. The cross section of the shapes resembles the crescent moon described by Lu *et al.*, but they are different due to the three dimensional cylindrical symmetry of the fibers used as templates. The cross-section of the tube walls shows a columnar structure typical of thin films deposited under the process conditions described in previous paragraphs.

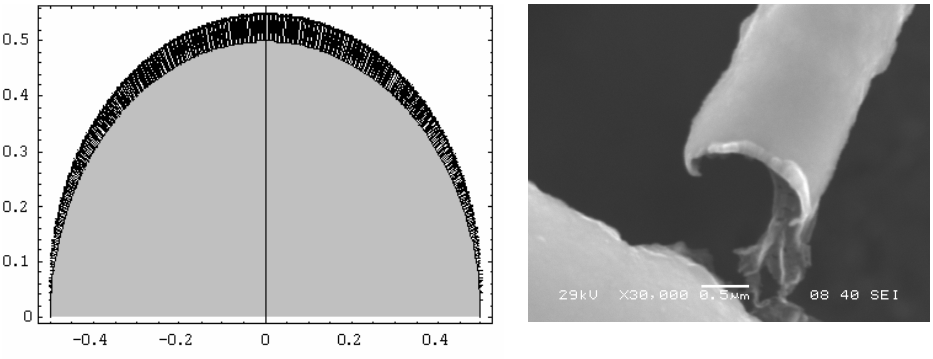

(a) (b)

Fig. 6. (a) Simulation of the thickness of the palladium coating (in black) deposited on top of a 1μm diameter fiber, and (b) micrograph of a morphological structure with a shape similar to that predicted by the model.

From the simulation, it can be seen that the deposition on a substrate with a cylindrical shape results in a non-uniform deposition where the minimum thickness is obtained at the surface element areas with angle α = 90°. For the surface elements with α > ±90° a more detailed analysis is needed, but it can be easily argued that geometrical shadowing from the top of the fiber will prevent any significant deposition of material. There are two conditions that will affect this non-uniform deposition and need to be considered. The first one is the scattering of palladium atoms being sputtered from the target as they travel toward the substrate, which produces a broader distribution of incoming angles at the fiber surface and is expected to reduce the non-uniformity in thickness at the surface. The second one is

bombardment-induced diffusion of palladium on the surface of the fiber. The fact that the entire fiber surface will be coated, if enough deposition time is allowed, shows that these two effects are relevant even when the deposition conditions were chosen to reduce their effect. An example is shown in Fig. 7 where the amount of time, 2 ks, allows for the deposition of enough Pd to coat all the surface of the fiber and, after the template is removed, the shape of a hollow cylinder is created. The fact that thicknesses of sections of the cylinder walls are not equal results from the asymmetry in the line-of-sight deposition. The fibers in Fig. 7 show thorn-like features outgrowing preferentially from the sides of the fibers. A careful examination will show that the thorns-like features have facets suggesting that they are Pd crystals. An explanation of the outgrowth of these crystals towards the sides of the fiber, that are perpendicular to the incoming flux, will be published elsewhere and it will be shown that, although vapor scattering is significant, the mechanisms of shadowing and competitive growth on a curved substrate are responsible for the external shape morphology observed.

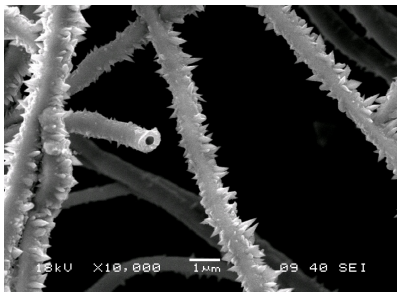

Fig. 7. A palladium cylinder is shown where the hollow interior is exposed. Notice the asymmetry in the wall thickness in sections of the cylinder as result of the line-of-sight deposition. The mean fiber diameter, previous to the Pd deposition, was 250 nm.

5 CONCLUSIONS

Palladium was deposited on top of polymer fibers that acted as templates to shape specific morphological structures. The deposition pressure and substrate temperature were adjusted to produce low adatom-mobility conditions resulting in the formation of specific shapes defined by the arrival of material on the geometrical configuration of the template surface. More material is deposited on top of the fibers than on the sides or bottom, and the thickness asymmetry can be modeled in terms of a cosine dependence on the angle at each surface area element. The shape of the morphological structures created, after being released from the template by the heat treatment, will depend on the amount of palladium being deposited. For small deposition times, the thickness of the wall does not provide enough support to maintain the mechanical integrity of the half tube deposited on top of the fiber, and when it is released it takes the shape of a ribbon. For longer deposition times, the shape that mimics the top half of the fiber is maintained in the form of a half tube and resembling a crescent moon in cross-section. As the deposition times keep increasing the thickness of the walls increases and a larger portion of the bottom part is covered until a hollow cylinder is created.

For small amounts of time, less than about 120 s, the thickness of the walls of the ribbons and half tubes is less than 100 nm in the middle top and decreases toward cero at the edges. The walls, with the cross-section shape of a crescent moon, are composed of nanoscale columns typical of thin films, as shown in Fig. 6(b), and the crystalline structure is also at the nanoscale level. It can be argued that the ribbons and half tubes have three types of structures

at the nanoscale level; their external shape, the columnar shape and their crystallinity. All of them can be modified by controlling process parameters in the sputtering and electrospinning techniques. Our ability to control the shape of the features of metal nanostructures will allow us to study their effect in future photonics applications.

Acknowledgment

The authors appreciate the leadership, the ideas and the enthusiasm that Russ Messier has provided to the scientific community and will like to congratulate him in his 65th birthday. They also acknowledge the support of NSF-DMR-0353730 and NIH-MD-001112D grants in different aspects of this project.

References

[1] B. A. Movchan and A. V. Demchishin, "Study of the structure and properties of thick vacuum condensates of nickel, titanium, tungsten, aluminum oxide, and zirconium dioxide," *Phys. Met. Metallogr.* **28**, 83-90 (1969).

[2] J. A. Thorton, "Influence of apparatus geometry and deposition conditions on the structure and topography of thick sputtered coatings," *Ann. Rev. Mater. Sci*. **7**, 239-260 (1977) [doi:10.1146/annurev.ms.07.080177.001323].

[3] R. Messier, A. P. Giri, and R. A. Roy, "Revised structure zone model for thin film physical structure," *J. Vac. Sci. Technol. A* **2**(2), 500-503 (1984) [doi:10.1116/1.572604].

[4] R. Messier, "Toward quantification of thin film morphology," *J. Vac. Sci. Technol. A* **4**(3), 490-495 (1986) [doi:10.1116/1.573866].

[5] R. Messier and J. E. Yehoda, "Geometry of thin-film morphology," *J. Appl. Phys.* **58**, 3739-3746 (1985) [doi:10.1063/1.335639].

[6] R. Messier, T. Gehrke, C. Frankel, V.C. Venugopal, W. Otaño, and A. Lakhtakia, "Engineered sculptured nematic thin films," *J. Vac. Sci. Technol. A* **15**(4), 2148-2152 (1997) [doi:10.1116/1.580621].

[7] A. Rodriguez-Navarro, W. Otaño-Rivera, J. M. García-Ruiz, R. Messier, and L. J. Pilione, "Preparation of highly oriented polycrystalline AlN thin films deposited on glass at oblique-angle incidence," *J. Mater. Res.* **12**(7), 1689-1692 (1997) [doi:10.1557/JMR.1997.0232].

[8] R. Messier, V. C. Venugopal, and P. D. Sunal, "Origin and evolution of sculptured thin films," *J. Vac. Sci. Technol. A* **18**, 1538-1545 (2000) [doi:10.1116/1.582381].

[9] A. Lakhtakia and R. Messier, *Sculptured Thin Films: Nanoengineered Morphology and Optics*, SPIE Press, Bellingham, WA (2005).

[10] Morphology, in Merrian-Webster Dictionary online, Retrieved from http://www.merriam-webster.com/ (August, 2008).

[11] F. C. Frank, "Foreword," in *Morphology of Crystals,* Ichiro Sunagawa, Ed., Terra Scientific, Tokyo (1987).

[12] S. Niwa, M. Eswarmoorthy, J. Nair, S. Raj, N. Itoh, H. Shoji, T. Nomba, and F. Mizukami, "A one-step conversion of benzene to phenol with a palladium membrane," *Science* **295**, 105-107 (2002) [doi:10.1126/science.1066527].

[13] S. W. Kim, M. Kim, W. Y. Lee, and T. J. Hyeon, "Fabrication of hollow palladium spheres and their successful application to the recyclable heterogeneous catalyst for Suzuki coupling reactions," *J. Am. Chem. Soc*. **124**, 7642-7643 (2002)[doi:10.1021/ja026032z].

[14] H. Wipf, *Hydrogen in Metals III*, Springer, Berlin (1997) [doi: 10.1007/BFb0103398].

[15] F. Favier, E. C. Walter, M. P. Zach, T. Benter, and R. M. Penner, "Hydrogen sensors and switches from electrodeposited palladium mesowire arrays," *Science* **293**, 2227-2231 (2001) [doi:10.1126/science.1063189].

[16] E. C. Walter, F. Favier, and R. M. Penner, "Hydrogen sensors and switches from electrodeposited palladium mesowire arrays," *Anal. Chem.* **74**, 1546-1553 (2002) [doi:10.1021/ac0110449].

[17] Z. Shi, S. Wu, and J. A. Szpunar, "Synthesis of palladium nanostructures by spontaneous electroless deposition," *Chem. Phys. Lett.* **422**, 147-151 (2006) [doi:10.1016/j.cplett.2006.02.065].

[18] M. Z. Atashbar, V. Bliznyuk, D. Banerji, and S. Singamaneni, "Deposition of parallel arrays of palladium nanowires on highly oriented pyrolitic graphite," *J. All. Comp.* **372**, 107-110 (2004) [doi:10.1016/j.jallcom.2003.10.014].

[19] C. L. Tien, H. W. Chen, W. F. Liu, S. S. Jyu, S. W. Lin, and Y. S. Lin, "Hydrogen sensor based on side-polished fiber Bragg gratings coated with thin palladium film," *Thin Sol. Films* **516**, 5360-5363 (2008) [doi:10.1016/j.tsf.2007.07.045].

[20] J. W. Elam, A. Zinivev, C. Y. Han, H. H. Wang, U. Welp, J. N. Hryn, and M. J. Pellin, "Atomic layer deposition of palladium films on Al2O3 surfaces," *Thin Sol. Films* **515**, 1664-1673 (2006) [doi:10.1016/j.tsf.2006.05.049].

[21] F. A. Lewis, *The Palladium Hydrogen System*, Academic Press, New York (1967).

[22] M. Steinhart, Z. Jia, A. K. Schaper, R. B. Wehrspohn, U. Gosele, and J. H. Wendorff, "Palladium nanotubes with tailored wall morphologies," *Adv. Mater.* **15**, 706-709 (2003) [doi:10.1002/adma.200304502].

[23] W. D. Westwood, *Sputter Deposition*, Am. Vacuum Soc. Education Committee Book Series, New York (2003).

[24] T. Unagami, A. Lousa, and R. Messier, "Silicon thin film with columnar structure formed by rf diode sputtering," *Jpn. J. Appl. Phys*. **36**, L737-L739 (1997) [doi:10.1143/JJAP.36.L737].

[25] D. A. Czaplewski, S. S. Verbridge, and H. G. Craighead, "Nanomechanical oscillators fabricated using polymeric nanofiber templates," *Nano Lett.* **4**, 437-439 (2004) [doi:10.1021/nl035149y].

[26] O. Sánchez, M. Hernández-Vélez, D. Navas, M. A. Auger, J. L. Baldonedo, R. Sanz, K. R. Pirota, and M. Vázquez, "Functional nanostructured titanium nitride films obtained by sputtering magnetron," *Thin Sol. Films* **495**, 149-153 (2006) [doi:10.1016/j.tsf.2005.08.203].

[27] M. Feng and R. J. Puddephatt, "Chemical vapor deposition of macroporous platinum and palladium-platinum alloy films by using polystyrene spheres as templates," *Chem. Mater*. **15**, 2696-2698 (2003) [doi:10.1021/cm034170x].

[28] M. Bognitzki, Z. Jia, A. K. Schaper, R. B. Wehrspohn, U. Gösele, and J. H. Wendorff, "Polymer, metal, and hybrid nano- and mesotubes by coating degradable polymer template fibers (TUFT process)," *Adv. Mater.* **12**, 637-640 (2000)[doi:10.1002/(SICI)1521-4095(200005)12:9<637::AIDADMA637>3.0.CO;2-W].

[29] Y. Lu, G. L. Liu, J. Kim, Y. X. Mejia, and L. P. Lee, "Nanophotonic crescent moon structures with sharp edge for ultrasensitive biomolecular detection by local electromagnetic field enhancement," *Nano Lett.* **5**, 119-124 (2005) [doi:10.1021/nl048232+].

[30] D. Li and Y. Xia, "Electrospinning of nanofibers: reinventing the wheel?," *Adv. Mater.* **16**, 1151-1170 (2004) [doi:10.1002/adma.200400719].

[31] W. Otaño, A. Otero, J. M. Otaño, C. S. Otaño, J. J. Santiago, and V. M. Pantojas, "Formation of palladium structures combining electrospinning and dc sputtering," *Mater. Res. Soc. Symp. Proc.* **948E**, 0948-B05-12 (2007).
[32] Y. Wang, M. Aponte, N. Leon, I. Ramos, R. Furlan, S. Evoy, and J. J. Santiago, "Synthesis and characterization of tin oxide microfibres electrospun from simple precursor solution," *Semicond. Sci. Technol.* **19**, 1057-1060 (2004) [doi:10.1088/0268-1242/19/8/017].
[33] Joint Committee on Powder Diffraction Studies (JCPDS) card No. 46-1043.
[34] R. J. Gnaedinger, "Some calculations of thickness distribution of films deposited from large area sputtering sources," *J. Vac. Sci. Technol*. **6**, 355-362 (1969) [doi:10.1116/1.1492693].

Víctor M. Pantojas is an associate professor at the University of Puerto Rico at Cayey. He received his BS degree in physics from the University of Puerto Rico, Río Piedras Campus in 1987 and his MS and PhD degrees in Solid State Physics from the Rensselaer Polytechnic Institute in 1991 and 1993, respectively. He is also in charge of the XRD facilities at the Materials Characterization Center.

Diego Rodríguez is a PhD candidate of the Chemical Physics Program of the University of Puerto Rico at Río Piedras where he received his MS degree in physics in 2007. He finished his BS at the University of Costa Rica in 2000.

Gerardo Morell is a full professor at the University of Puerto Rico at Río Piedras. He received his BS and MS degrees in physics from the University of Puerto Rico, Río Piedras Campus in 1989 and 1994, respectively, and his PhD degree in Chemical Physics in 1995. He is also a member of the Institute for Functional Nanomaterials.

Adamari Rivera received her BS in Chemistry at the University of Puerto Rico at Cayey in 2008. She is an employee of a pharmaceutical company.

Carlos Ortiz is an associate professor at the University of Puerto Rico at Cayey. He received his BS degree in physics from the University of Puerto Rico, Río Piedras Campus in 1979 and his MS and PhD degrees in Physics from the University of New York at Albany in 1991 and 1993, respectively.

Jorge J. Santiago-Avilés is an associate professor at the University of Pennsylvania. He received his BS from the University of Puerto Rico, Río Piedras Campus in 1966, and his PhD from the Pennsylvania State University in 1971.

Wilfredo Otaño is a full professor at the University of Puerto Rico at Cayey. He received his BS and MS degrees in physics from the University of Puerto Rico, Río Piedras Campus in 1979 and 1983, respectively, and his PhD degree in Materials from Pennsylvania State University in 1998. He is also a member of the Institute for Functional Nanomaterials.